




Article

Microstructural Characteristics of 3Y-TZP Ceramics and Their Effects on the Flexural Strength

Manuel Fellipe Rodrigues Pais Alves ^{1,*} , Leonardo Queiroz Bueno de Campos ¹, Bruno Galvão Simba ², Cosme Roberto Moreira da Silva ³ , Kurt Strecker ⁴ and Claudinei dos Santos ^{1,5} 

¹ Faculdade de Tecnologia de Resende, Universidade do Estado do Rio de Janeiro, UERJ-FAT, Rodovia Presidente Dutra, km 298, Resende 27537-000, RJ, Brazil

² Faculdade de Engenharia de Guaratinguetá, Universidade Estadual Paulista, UNESP/FEG, Av. Ariberto Pereira da Cunha, 333, Portal das Colinas, Guaratinguetá 12516-410, SP, Brazil

³ Faculdade de Tecnologia, Universidade de Brasília, UNB, Asa Norte, Brasília 70910-900, DF, Brazil

⁴ Department of Mechanical Engineering, Universidade Federal de São João Del'Rei—UFSJ, Pça Frei Orlando 170, Sao joao del-Rei 36307-352, MG, Brazil

⁵ Escola de Engenharia Industrial Metalúrgica de Volta Redonda (EEIMVR), Universidade Federal Fluminense (UFF), Av. Trabalhadores, 420, Vila Santa Cecília, Volta Redonda 27255-125, RJ, Brazil

* Correspondence: manuel.alves@ua.pt

Abstract: This work evaluates the effects of grain growth and tetragonality of the *t*-ZrO₂ phase on the mechanical properties of 3Y-TZP ceramics. Samples were sintered at 1475 °C for 2 h, and at 1600 °C for 2, 12, or 24 h. After sintering, the tetragonal ZrO₂ polytypes *t* and *t'* were observed under all sintering conditions, while a residual content of monoclinic ZrO₂ was detected in samples sintered at 1600 °C for 24 h. The average grain size was found to vary from 0.65 ± 0.10 to 2.20 ± 0.35 μm. Moreover, zirconia ceramics sintered at 1475 °C for 2 h exhibit higher flexural strength (1210 ± 85 MPa), while samples sintered at 1600 °C for 24 h exhibit the lowest flexural strength (910 ± 90 MPa). These results were related to the progressive formation of Y³⁺-rich grains (*t'*-ZrO₂) due to the grain boundary segregation-induced phase (GBSIPT) mechanism. Due to the high stabilizer concentration in the solid solution, these grains present lower tetragonality, being highly stable at room temperature. Consequently, the observed strength reduction of samples sintered at 1600 °C for 24 h is related to the presence of the *t'*-ZrO₂ phase, which is less prompt to the phase transformation toughening process, limiting shielding zones' effectiveness at the crack tip.

Keywords: Y-TZP; mechanical properties; microstructure; tetragonality; phase transformation



Citation: Alves, M.F.R.P.; de Campos, L.Q.B.; Simba, B.G.; da Silva, C.R.M.; Strecker, K.; dos Santos, C. Microstructural Characteristics of 3Y-TZP Ceramics and Their Effects on the Flexural Strength. *Ceramics* **2022**, *5*, 798–813. <https://doi.org/10.3390/ceramics5040058>

Academic Editor: Margarita A. Goldberg

Received: 5 September 2022

Accepted: 11 October 2022

Published: 17 October 2022

Publisher's Note: MDPI stays neutral with regard to jurisdictional claims in published maps and institutional affiliations.



Copyright: © 2022 by the authors. Licensee MDPI, Basel, Switzerland. This article is an open access article distributed under the terms and conditions of the Creative Commons Attribution (CC BY) license (<https://creativecommons.org/licenses/by/4.0/>).

1. Introduction

Ceramics based on yttria-stabilized zirconia, ZrO₂-Y₂O₃ (Y-TZP), are polycrystalline ceramics with significant technological applications due to their excellent mechanical properties, such as high flexural strength and fracture toughness [1,2]. Under atmospheric pressure, ZrO₂ exhibits three distinct crystalline phases depending on temperature: monoclinic (from room temperature up to 1170 °C), tetragonal (between 1170 and 2180 °C), and cubic (above 2180 °C) [3]. The instability of the tetragonal polymorph at room temperature gives rise to a spontaneous transformation during cooling. This tetragonal to monoclinic (*t*→*m*) transformation is followed by a volumetric expansion of about 4–5 vol.%, generating residual stresses which degrade its solid structure. However, adding oxides of the MO-, MO₂-, or M₂O₃-type to ZrO₂-based ceramics makes it possible to stabilize the high-temperature polymorphs (tetragonal or cubic) at room temperature. This stabilization occurs through the change of oxygen vacancies, promoted by the substitutional solid solution of these oxides in the ZrO₂ unit cell. Polycrystalline tetragonal zirconia stabilized with 3 mol% yttria (3Y-TZP) is an example in which the metastable tetragonal phase is induced. In these materials, the martensitic transformation *t*→*m* only occurs if a free energy

barrier is overcome, such as by stress fields arising from applied external stresses [4,5]. The mechanism inhibits the propagation of cracks by inducing compressive stresses around the crack during its propagation. Some authors propose a resulting stress of approximately 38 MPa per volume percent fraction of the transformed monoclinic phase [6]. Furthermore, the amount of yttria in the ZrO_2 solid solution is an important parameter. It affects several parameters, such as the phase composition, the average grain size, the martensitic transformation temperature, the degradation resistance, and the resulting mechanical properties. Previous research [7] evaluated, with the aid of EDS nanoprobe [8], the distribution of Y^{3+} ions in the microstructure of 3Y-TZP ceramics. The increase in temperature or sintering time leads to a segregation of Y^{3+} ions in the grain boundaries, mainly in the triple junctions, giving rise to the formation and thickening of peripheries, rich in Y^{3+} , which are the preferred regions for the stabilization of the ZrO_2 -cubic phase [7–9]. Yashima et al. [10] developed metastable–stable phase diagrams for zirconia stabilized with different oxides. The authors proposed a correlation between the yttria concentration in the unit cell with the relation of the c/a lattice parameter, verifying the existence of three possible forms for a metastable tetragonal phase:

- The transformable metastable tetragonal phase, called t , is of great interest for structural applications as it presents a martensitic transformation ($t \rightarrow m$) when subjected to stress, providing excellent mechanical strength results due to the phase transformation toughening mechanism [3].
- The metastable tetragonal phase, called t' , which, due to its high concentration of stabilizer in solution, has lower tetragonality, being extremely stable at room temperature, and does not undergo the martensitic transformation ($t \rightarrow m$) under mechanical stress.
- The metastable tetragonal phase, called t'' . This third and particular form of the tetragonal phase has been identified by Raman spectroscopy or neutron diffraction, taking into account that X-ray diffraction cannot distinguish the small variations between the lattice parameters of this phase and the ZrO_2 -cubic phase since the tetragonality relation points to a $c/a\sqrt{2}$ ratio close to unity. Based on available literature data, Viazzi et al. [11] proposed limits for the stability domains of the different forms of the ZrO_2 -tetragonal phase as a function of their lattice parameters, as shown in Figure 1.

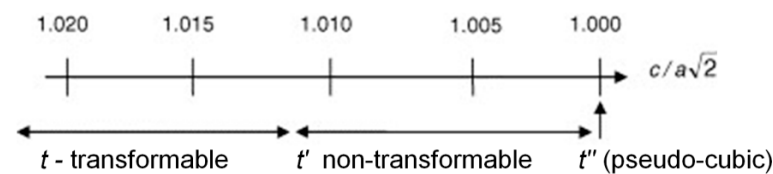


Figure 1. The tetragonal forms of Y-TZP as a function of the tetragonality and transformability (adapted from Viazzi et al. [11]).

The average grain size of the sintered zirconia is a factor directly related to the sintering conditions and greatly impacts the stability of the ZrO_2 -tetragonal phase, which in turn affects the mechanical properties of 3Y-TZP ceramics. Shukla et al. [12] reviewed the mechanism of meta-stabilization of t - ZrO_2 in nanocrystalline (100 nm), sub-micrometer (0.1–1 μm), and micrometer (>1 μm) scales, considering models based on free energy analysis, lattice defects, and residual stresses, among others.

For materials with sub-micrometric and micrometric grain sizes, it is considered that ZrO_2 -tetragonal can be stabilized at room temperature only if the average radius of the grains present in the microstructure is below the critical radius for transformation, explained by the thermodynamic description for the stress-induced transformation. Equation (1) describes the critical radius for spontaneous transformation:

$$r_c = -3\Delta\sigma_{m \rightarrow t} / (\Delta\Psi_{m \rightarrow t} + \Delta\varepsilon_{m \rightarrow t}) \quad (1)$$

where: " r_c " = critical radius for spontaneous transformation (nm), " $\Delta\sigma_{(m\rightarrow t)}$ " = variation of surface free energy between a ZrO₂-tetragonal and ZrO₂-monoclinic grain (J/m²), " $\Delta\Psi_{(m\rightarrow t)}$ " = free energy change in volume between a ZrO₂-tetragonal and ZrO₂-monoclinic grain (J/m²), and " $\Delta\varepsilon_{(m\rightarrow t)}$ " = variation of residual stress between a ZrO₂-tetragonal and ZrO₂-monoclinic grain (J/m²).

The data proposed by Shukla et al. [12] are consistent with the surveys carried out by Shahmiri et al. [13] and Zhang [14], indicating that grains with an average size of less than 100 nm have great thermodynamic metastability, likely to remain stable, even when exposed to a stress field caused by the propagation of a crack and thus inhibiting the toughening mechanism by martensitic transformation. On the other hand, grains with an average size greater than 1 μm tend not to have the thermodynamic metastability necessary to retain the crystal structure of the tetragonal phase at room temperature, therefore leading to a spontaneous transformation of the grains during cooling.

Based on these data, the main processing parameters which must be controlled during the manufacturing of Y-TZP ceramics are (i) homogeneity of composition and the particle size of the starting powder, and (ii) sintering conditions (heating rate, temperature, and isotherm (dwell time)) [15]. Furthermore, the sintering parameters directly influence densification and microstructure of the zirconia ceramics [16], and consequently, strongly affect the mechanical strength.

Previous works [17,18] report the effect of the zirconia grain size on their flexural strength as a direct function of the average grain size of sintered Y-TZP ceramics. However, a gap exists in the literature regarding the constitution of a dual-phase microstructure formed by transformable and not transformable grains, subject to different grain growth kinetics. Therefore, this work developed dense Y-TZP-based ceramics with significant variations in the average grain size and the tetragonal/cubic ZrO₂ ratio, using sintering temperatures between 1400 and 1600 °C. In addition, the flexural strength was evaluated, and the results were correlated with critical defect size, residual porosity, tetragonal ZrO₂ grain population, and the t→m martensitic phase transformation.

2. Materials and Methods

2.1. Processing

This work used a high-purity commercial zirconia powder, stabilized with 3 mol.% of yttria (Zpex, Tosoh Corp, Tokyo, Japan), to manufacture the specimens. Specimens ($n > 110$) with dimensions of $\text{Ø } 14 \times 1.5$ mm, following the recommendation of ISO 6872-15 [19] standard, were produced by uniaxial compaction under a pressure of 100 MPa for 30 s and subsequent sintering at temperatures ranging from 1400 to 1600 °C, with an isothermal holding time of 2 h, in an electrical furnace with MoSi₂ heating elements (MAITEC® F1650, São Carlos, SP, Brazil) with heating and cooling rates of 5 °C/min. Furthermore, samples were sintered at 1600 °C with different isothermal holding times of 2, 12, and 24 h.

2.2. Sample Characterizations

The apparent density of the 3Y-TZP sintered samples was determined using Archimedes' principle, and the relative density of the bulk was obtained by relating the apparent density with its real density (6.047 g·cm⁻³), determined by He-pycnometry (Ultrapyc 5000 Micro, Anton Paar, Graz, Austria).

X-ray diffractometry was used to identify the crystalline phases present in the samples using the PANalytical-Empyrean diffractometer (Malvern PANalytical, Worcestershire, UK), equipped with a Cu-K α radiation source (1.5405 Å) and a PIXcel 3D detector, programmed to perform scans within the 2 θ range of 10 to 90°, with a step width of 0.01° and a counting time of 100 s. The diffractograms obtained were compared with a standard crystallographic information file (CIF) from the Inorganic Crystallographic Structures Database (ICSD). To compare the diffraction patterns obtained with the reference catalog file, the X'pert Highscore plus program (Malvern PANalytical, Worcestershire, UK), was used.

Refinements of the crystalline structure and quantitative determination of the phases present were carried out by the Rietveld method [20], using the FullProf program, developed by Rodríguez-Carvajal et al. [21]. Considering the difficulty in identifying and refining zirconia polymorphs, the model proposed by Krogstad et al. [22] was used. The model considers the variation of the lattice parameters of the ZrO₂-tetragonal and ZrO₂-cubic phases as a function of the percentage of yttria present in the phase, using the total amount of yttria present in the starting powder as a limiting parameter.

The authors verified the existence of tetragonal phases with different degrees of tetragonality, consistent with previous reports in the literature [22–24] up to a condition where $c/a\sqrt{2} \approx 1$, in which the tetragonal structure presents a percentage of yttria and a degree of tetragonality consistent with a cubic structure. The data disclosed by Krogstad et al. [22] have been used by several high-impact studies in the literature [25–30] to determine the percentage of yttria in the analyzed phases and to adjust the quantified phase fractions as a function of the total yttria present in the composition. For this reason, the lattice parameters refined using the Rietveld method were later analyzed using the model proposed by Krogstad et al. [22], based on Equations (2)–(5):

$$a_t\sqrt{2} = 5.07987 + 3.857 \cdot 10^{-3} [\text{YO}_{1.5}] \quad (2)$$

$$c_t = 5.19772 - 3.771 \cdot 10^{-3} [\text{YO}_{1.5}] \quad (3)$$

$$a_c = 5.11742 + 1.559 \cdot 10^{-3} [\text{YO}_{1.5}] \quad (4)$$

$$\text{Tetragonality} = \frac{c}{a_t\sqrt{2}} = 1.02311 - 1.498 \cdot 10^{-3} [\text{YO}_{1.5}] \quad (5)$$

where: “ a_t ” = lattice parameter “ a ” of the ZrO₂-tetragonal phase, “ c_t ” = lattice parameter “ c ” of the ZrO₂-tetragonal phase, “ a_c ” = lattice parameter “ c ” of the ZrO₂-cubic phase, and YO_{1.5} = percentage in mol of yttrium oxide (Y₂O₃) present in the phase—note the stoichiometry.

After sintering, both specimen surfaces were grounded and polished using 9, 6, and 1 μm diamond suspensions. The polished specimens were cleansed in acetone and isopropyl alcohol in an ultrasonic bath for 10 min. The samples were then thermally etched at 1450 °C for 20 min with a heating and cooling rate of 25 and 10 °C/min, respectively, and sputtered with gold.

The microstructures of the sintered samples were observed by scanning electron microscopy (SEM-FIB) (JSM 7100FT, JEOL, Tokyo, Japan) microscope, with a secondary electron detector. The grain size distributions of the sintered samples were determined using the software IMAGE J (National Institute of Mental Health, Bethesda, MD, USA) for SEM micrographs. All micrographs were pre-processed with filters to minimize imperfections such as noisy pixels, inadequate contrast, and brightness. The mean grain size was determined as the Feret diameter of the grains. For statistical reasons, a grain size of at least 1000 grains of each sample was measured to calculate the average grain size.

2.3. Mechanical Properties

Young’s moduli were measured by the Impulse Excitation Technique (IET) using a Sonelastic[®] apparatus (ATCP, São Carlos, Brazil). The impeller consists of a steel ball of 5.5 mm in diameter glued to a flexible polymer rod. The specimens (discs of 14 mm in diameter) were struck elastically on an anti-nodal point to excite the sample and the induced vibrations were recorded by a microphone. The measurements were repeated until five similar consecutive readings, with a variation of less than 2 Hz, were obtained. Young’s moduli were calculated using the ASTM E1876 [31] standard, based on the theory of free vibrations of elastic bodies.

Fracture toughness was determined by the Vickers indentation method, using the mathematical models proposed by Niihara et al. [32] and Shetty et al. [33]. As demonstrated by Coric et al. [34], these are the most suitable models for Y-TZP when the indentations are

carried out with loads less than or equal to 29.42 N and, consequently, generate Palmqvist type cracks. Equations (6) and (7) describe, respectively, the approaches proposed by Niihara et al. and Shetty et al. [32,33]:

$$K_c = 0.035 \left(\frac{l}{a}\right)^{-\frac{1}{2}} \left(\frac{H_v}{E\Phi}\right)^{\frac{-2}{5}} \left(\frac{H_v a^{\frac{1}{2}}}{\Phi}\right) \tag{6}$$

$$K_c = 0.0319 \cdot \frac{F}{a \cdot l^{\frac{1}{2}}} \tag{7}$$

where: K_c is the fracture toughness ($\text{MPa}\cdot\text{m}^{-0.5}$), “ c ” is the length of the crack, measured from the center of the indentation until the crack tip (μm), “ l ” is the length of the crack, measured from the tip of the indentation until the tip of the crack (μm), “ a ” is the half-length of the indentation diagonal (μm), “ H_v ” is the Vickers hardness (GPa), “ E ” is Young’s modulus (GPa), and “ Φ ” is a dimensionless constant developed by Niihara et al. [32] which can range between 2.7 and 3.

The biaxial flexural strength was measured in a piston-on-three-ball test using a universal testing machine, EMIC 1000 INSTRON-Group, Brazil, according to the ISO 6872-15 standard [19]. Each disc was positioned centrally on three steel balls (diameter of 3 mm, set equally apart on a supporting circle with a diameter of 10 mm). The polished surface of the specimen was positioned in the tensile stress zone, while the other surface was loaded with a ball punch (diameter 1.4 mm) with a crosshead speed of 0.5 mm/min until fracture. A thin plastic-coated thick paper was placed between the specimen and the flattened ball piston to evenly distribute the load. The maximum flexural strength was calculated using Equations (8)–(10):

$$\sigma_f = \frac{-0.2387P(X - Y)}{b^2} \tag{8}$$

where:

$$X = (1 + \nu) \ln \left(\frac{r_2}{r_3}\right)^2 + [1 - \nu/2] \left(\frac{r_2}{r_3}\right)^2 \tag{9}$$

$$Y = (1 + \nu) \left[1 + \ln \left(\frac{r_1}{r_3}\right)^2 + (1 - \nu) \left(\frac{r_1}{r_3}\right)^2 \right] \tag{10}$$

where: “ σ_f ” is the maximum flexure strength (MPa), “ P ” is the rupture load (N), “ ν ” is the Poisson’s ratio, “ r_1 ” is the radius of the supporting circle (mm), “ r_2 ” is the radius of the loaded area (mm), “ r_3 ” is the specimen’s radius (mm), “ b ” is the specimen’s thickness (mm), and “ ν ” is the measured Poisson coefficient of 0.31.

2.4. Statistical Strength Analysis

The statistical evaluation of the biaxial flexural strength of the Y-TZP samples was realized using Weibull statistics. The two-parameter Weibull distribution function was used according to Equation (11):

$$P = 1 - \exp \left\{ \left[-\frac{\sigma}{\sigma_0} \right]^m \right\} \tag{11}$$

where: “ P ” is the failure probability, “ m ” is the Weibull modulus, “ σ_0 ” is the characteristic stress (MPa), and “ σ ” is the average bending strength (MPa).

Weibull parameters m and σ_0 are obtained by transforming Equation (11) into Equation (12) and plotting $\ln \left[\frac{1}{(1-P)} \right]$ versus $\ln \sigma$, as:

$$\ln \ln \left[\frac{1}{\left(\frac{1}{P}\right)} \right] = m \times \ln \sigma - m \times \ln \sigma_0 \tag{12}$$

The characteristic stress, " σ_0 ", which corresponds to a failure probability of 63.2%, was estimated as a reference compared to the average stress values. The Weibull modulus (m) and 95% confidence intervals (95%CI) were obtained by the maximum likelihood method [35].

A complementary statistical analysis of the results [36,37] was performed by the Student's t -test. First, one-way ANOVA was used to analyze the mechanical properties, followed by a Tukey's Honestly Significant Difference (HSD) post hoc test to analyze the biaxial flexural strength of the groups ($\alpha = 0.05$).

3. Results and Discussion

3.1. Densification, X-ray Diffraction, and Microstructure

Figure 2 presents the relative density as a function of the sintering temperature. It is observed that complete densification, close to 99.5%, was achieved for samples sintered above 1475 °C for 2 h. Based on these preliminary analyses, the samples used in the flexural strength analysis were sintered at 1475 °C for 2 h, and 1600 °C for 2, 12, or 24 h.

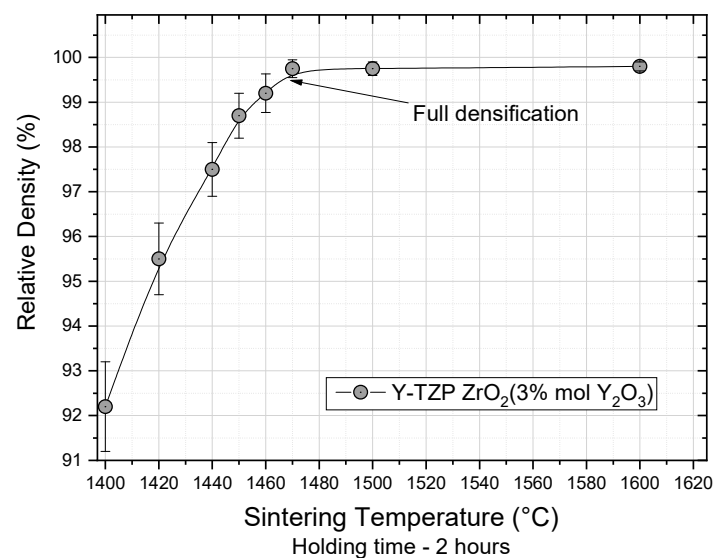


Figure 2. Relative density of sintered Y-TZP samples as a function of sintering temperature using an isothermal holding time of 2 h.

Figure 3 shows the phase analysis results by X-ray diffraction of the sintered samples according to the sintering conditions. The major crystalline phase identified is tetragonal t -ZrO₂, with different amounts of t' -ZrO₂ as a secondary phase under all sintering conditions. Table 1 presents the results of the refined lattice parameters, according to the proposed methodology, for the samples of 3Y-TZP sintered under different parameters.

The refinement of the identified crystalline structures (Table 1) showed a t -ZrO₂ tetragonal phase, with high tetragonality ($c/a\sqrt{2} > 1.015$ ratio), for all sintering conditions studied. According to data reported by Viazzi et al. [11], tetragonal structures with this degree of tetragonality tend to be transformable and therefore contribute to the optimization of the mechanical properties by the phase transformation toughening mechanism.

A trend of increasing tetragonality depending on the increase in temperature and sintering time from $c/a\sqrt{2} = 1.0157$ to 1.0167 has been observed. This trend is associated with the migration of yttria to the grain boundary regions, as Matsui et al. [28] proposed in their description of the phase nucleation mechanism in zirconia, GBSIPT. Furthermore, it is consistent with the data reported by Chevalier et al. [38] in their report on the effects of cubic phase nucleation on the mechanical properties of 3Y-TZP, since the amount of yttria measured for the t -ZrO₂ grains was reduced from 2.45 to 2.15 mol % between the extremes analyzed in this study.

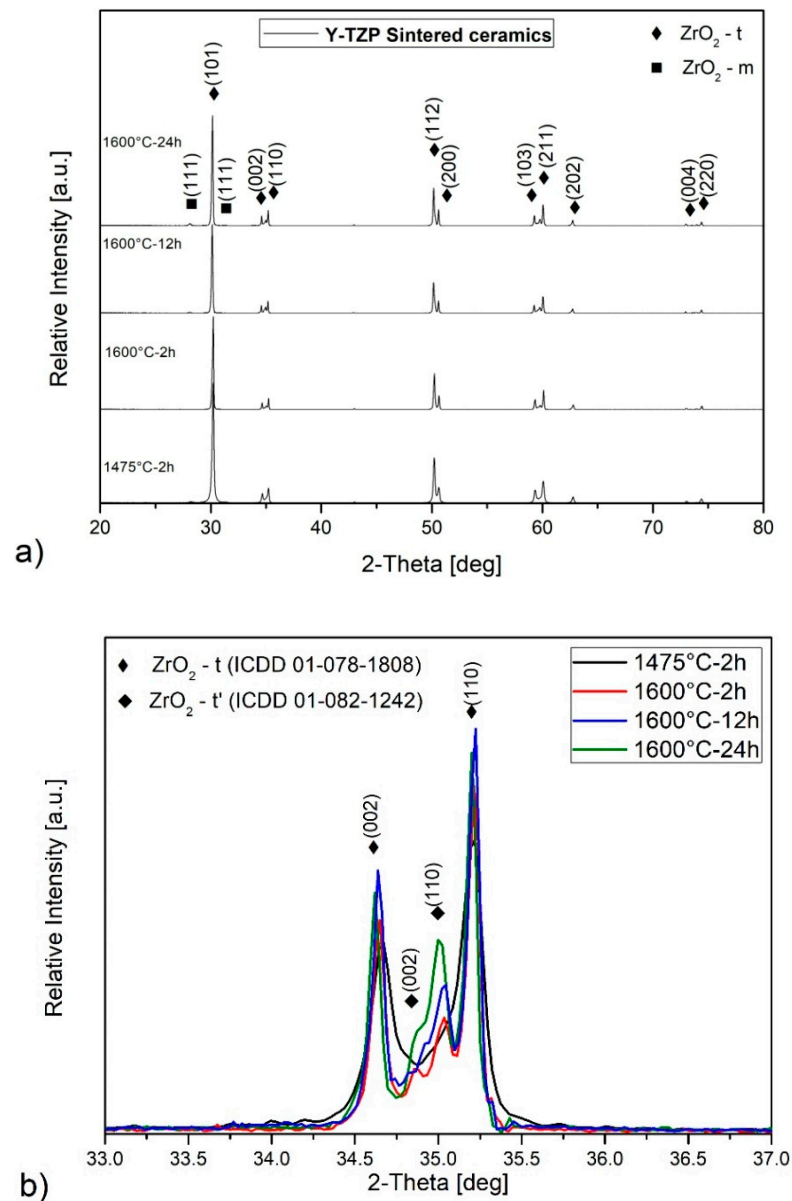


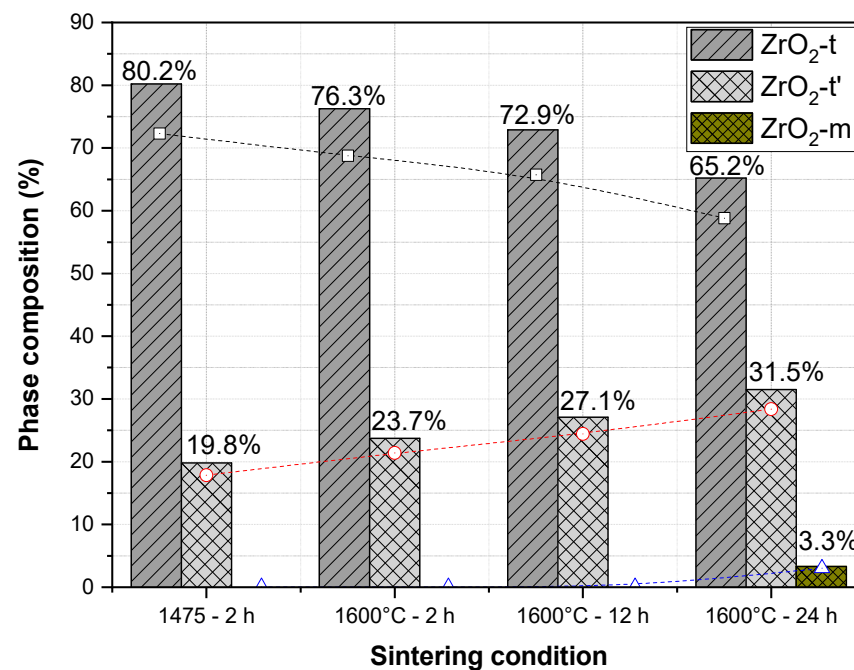
Figure 3. XRD patterns of the Y-TZP samples, sintered under different conditions, where: (a) full patterns of the polished samples, and (b) region of interest.

A secondary tetragonal phase (ZrO_2-t') of low tetragonality was also verified (see Table 1). The crystalline peaks for this phase were identified and adequately refined as the ZrO_2 -tetragonal phase (space group $P42/nmc$). However, the lattice parameters of this phase indicate a low tetragonality of $c/a\sqrt{2} \approx 1006$ for all samples analyzed, which is consistent with the data presented by Viazzi et al. [11] for non-transformable phase forms. Similar data have been reported by several other authors [10,11,39–41].

Although the ZrO_2-t phase was consistent with the $P42/nmc$ space group, the crystal structure exhibited only a slight deformation compared to the fluorite-type crystal structure, characteristic of the ZrO_2 -cubic phase. The literature confirms that this type of deformation is consistent with the variation in the volume of oxygen vacancies along the structure promoted by a high content of dopants. Although the concentration of Y_2O_3 measured for the ZrO_2-t' phase of approximately 5 mol.% is substantially higher compared to the concentration in the ZrO_2-t phase of about 2 mol.%, this content is still lower than that required for the stabilization of the cubic phase of 6.5 to 7 mol.%. Figure 4 presents the results of the quantitative phase analysis, in weight percentage, for the different sintering conditions.

Table 1. Refinement of 3Y-TZP crystal structure after sintering at different temperatures.

Lattice Parameters	1475 °C, 2 h	1600 °C, 2 h	1600 °C, 12 h	1600 °C, 24 h
ZrO ₂ -tetragonal (ZrO ₂ - <i>t</i>)	a = 3.605(2) Å	a = 3.604(2) Å	a = 3.603(1) Å	a = 3.603(1) Å
Space groups	c = 5.178(8) Å	c = 5.179(5) Å	c = 5.179(6) Å	c = 5.179(6) Å
P4 ₂ /nmc	V = 67.3113 Å ³	V = 67.283 Å ³	V = 67.243 Å ³	V = 67.255 Å ³
Relation between the lattice (c/a√2)	1.015(7)	1.016(2)	1.016(5)	1.016(7)
Y ₂ O ₃ in <i>t</i> -phase (mol.%)	2.45	2.32	2.21	2.15
ZrO ₂ -tetragonal' (ZrO ₂ - <i>t'</i>) (rich in yttria)	a = 3.622(7) Å	a = 3.623(0) Å	a = 3.621(5) Å	a = 3.624(0) Å
Space groups	c = 5.161(9) Å	c = 5.157(7) Å	c = 5.154(0) Å	c = 5.156(0) Å
P4 ₂ /nmc	V = 67.7445 Å ³	V = 67.701 Å ³	V = 67.59 Å ³	V = 67.716 Å ³
Relation between the lattice (c/a√2)	1.007 (5)	1.006 (6)	1.006 (3)	1.006 (0)
Y ₂ O ₃ in <i>t'</i> -phase (mol.%)	5.20	5.50	5.60	5.70

**Figure 4.** XRD crystallographic composition of the Y-TZP samples sintered under different conditions.

The results indicate that the ZrO₂-*t* phase is the majority phase for all sintering conditions studied. However, with increasing sintering time/temperature, a reduction of the amount of ZrO₂-*t* from about 80% to about 65% was observed. On the other hand, the material presents a slightly higher percentage of the ZrO₂-*t'* phase of about 5 wt.%, with a progressive increase in this phase, from 19.8% to 31.5%, probably generated by structural and morphological changes in the material. This change is likely to be caused by the metastability of this phase as a function of the decrease in the stabilizer concentration identified for the *t* and *t'*-ZrO₂ phases [7,28]. Furthermore, samples sintered at 1600 °C for 24 h show a small amount of monoclinic phase (ZrO₂-*m*) after sintering, originating from the spontaneous *t*→*m* transformation that occurs at 1100 °C [9]. However, other factors, such as the variation of the average grain size, will be considered for an adequate discussion of this subject.

Figures 5 and 6 show SEM micrographs of sintered Y-TZP samples and the results of the grain size distributions in samples sintered under different sintering parameters.

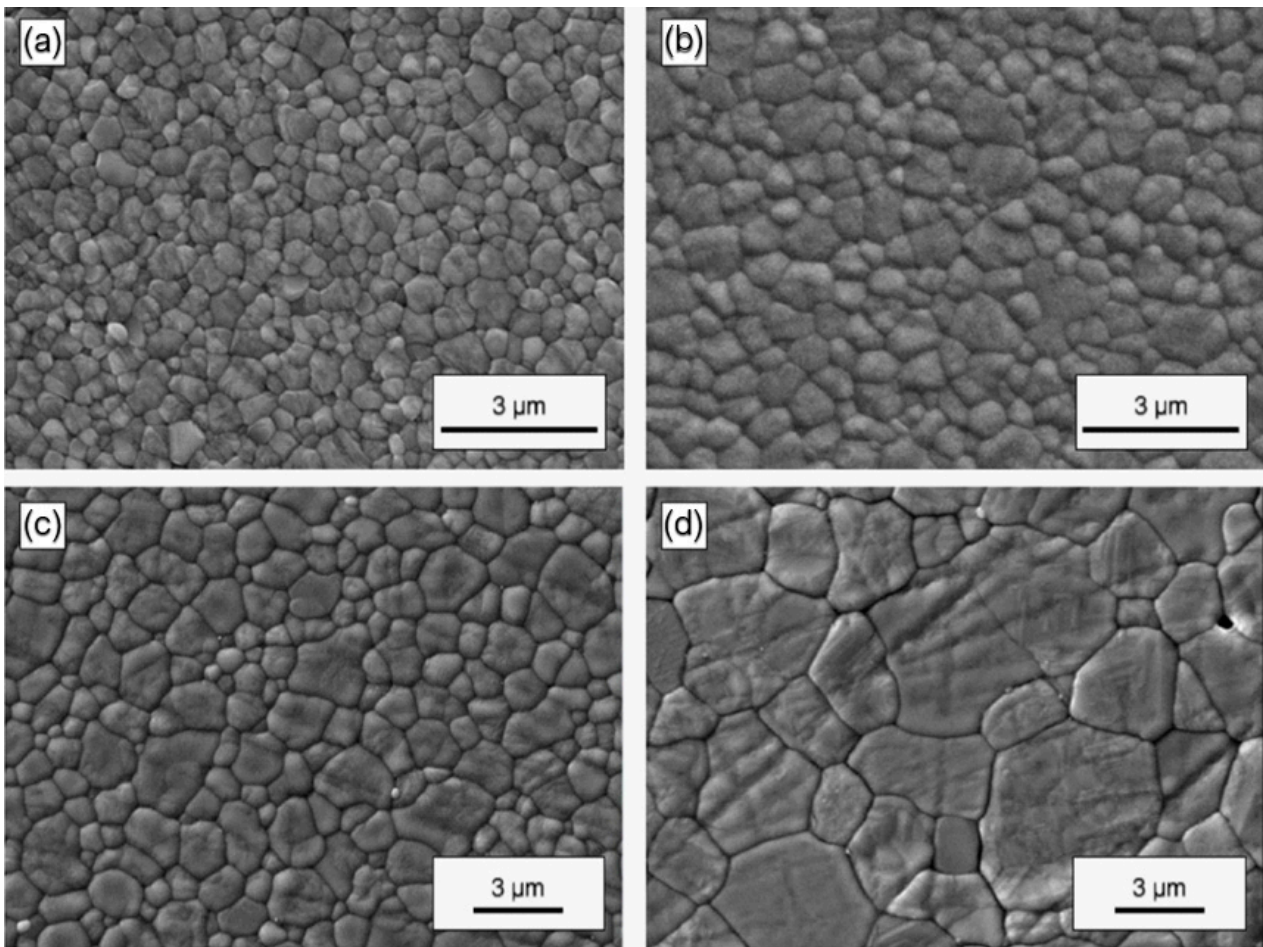


Figure 5. SEM micrographs of the Y-TZP samples sintered at different conditions: (a) 1475 °C for 2 h, (b) 1600 °C for 2 h, (c) 1600 °C for 12 h, and (d) 1600 °C for 24 h.

The results in Figure 6 indicate a considerable growth of zirconia grains as a function of temperature. The average grain size was found to vary from 0.65 ± 0.10 to 1.22 ± 0.19 μm with the increase in sintering temperature from 1475 to 1600 °C. Furthermore, the variation of the isothermal holding time in samples sintered at 1600 °C also resulted in considerable grain growth, with average sizes ranging from 1.22 ± 0.19 to 2.20 ± 0.35 μm .

The analysis of grain size distribution curves (Figure 6b) highlights that higher temperatures and longer dwell times lead to bimodal size distributions, with significant size variations, typical of TZP ceramics that show excessive growth of a specific group of zirconia grains. Previous studies [9,17] indicate that the group of larger grains within a 3Y-TZP ceramic is preferentially formed by grains of cubic or pseudo-cubic phase (t' or t''), which have a higher Y^{3+} content which favors their growth. The content of Y_2O_3 , or the concentration of Y^{3+} present in the stabilization of zirconia, changes its grain growth rate, as already demonstrated [9,17]. Thus, the preferential segregation of Y^{3+} in some grains and triple junctions promotes higher growth rates in these regions, resulting in substantial differences in grain sizes.

These morphological characteristics, combined with the results of X-ray diffraction that identified the presence of both phases (t - ZrO_2 and t' - ZrO_2) with different contents of Y_2O_3 in its composition, infer that the larger grains are, preferably, in the t' - ZrO_2 phase.

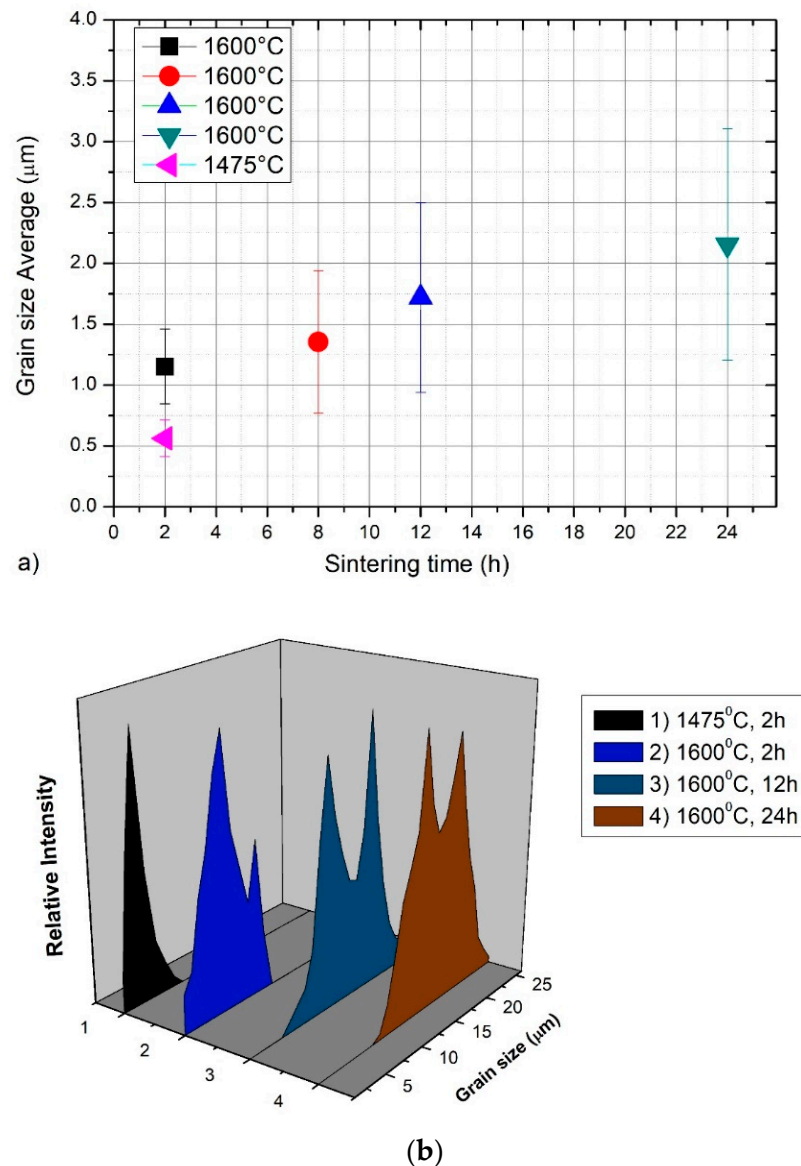


Figure 6. (a) Average size of zirconia grains as a function of the proposed sintering cycle. (b) Grain size distributions of sintered ZrO_2 .

3.2. Mechanical Properties

The results of the mechanical properties of elastic modulus, flexural strength, and fracture toughness are listed in Table 2.

Table 2. Mechanical properties of Y-TZP-based ceramics after sintering.

Sintering Conditions	Young's Modulus E (GPa)	Flexural Strength σ_f (MPa)	Fracture Toughness KIC (MPa.m ^{1/2}) **	Fracture Toughness KIC (MPa.m ^{1/2}) ***
1475 $^{\circ}\text{C}$, 2 h	189.2 \pm 3.5	1208 \pm 93	8.18 \pm 0.18	7.58 \pm 0.47
1600 $^{\circ}\text{C}$, 2 h	193.1 \pm 2.8	1015 \pm 136	7.48 \pm 0.47	8.32 \pm 0.52
1600 $^{\circ}\text{C}$, 12 h	194.3 \pm 2.4	947 \pm 70	7.17 \pm 0.44	7.47 \pm 0.45
1600 $^{\circ}\text{C}$, 24 h	198.8 \pm 3.6	922 \pm 116	6.89 \pm 0.33	7.23 \pm 0.51

* $n = 21/\text{group}$, ** Niihara model, *** Shetty model.

The results indicate that the elastic modulus increased slightly from 189.2 ± 3.5 to 198.8 ± 3.6 Gpa between the control group sintered at $1475\text{ }^\circ\text{C}$ for 2 h and the samples sintered at $1600\text{ }^\circ\text{C}$. The results can be considered statistically similar between the different groups. However, the slight increases observed can be correlated with a small increase in the relative density and t' phase. The fracture toughness values, in turn, do not present a well-defined profile as a function of the rise in temperature and isotherm level. There was a small increase in K_{IC} when the sintering temperature was increased to $1600\text{ }^\circ\text{C}$ for 2 h, which can be related to the increasing relative density. On the other hand, higher sintering levels lead to reductions in K_{IC} values, probably due to a decrease in the grain boundary population (density per unit area) due to grain growth and the amount of non-transformable zirconia grains.

The flexural strength results indicate a well-defined trend of decreasing values as a function of increasing temperature and dwell time. Samples from the control group, sintered at $1475\text{ }^\circ\text{C}$ for 2 h, showed σ_f of 1208 ± 93 MPa, while samples sintered at $1600\text{ }^\circ\text{C}$ for 24 h showed mean values of 922 ± 116 MPa, equivalent to a reduction of 24%. These results will be discussed later in terms of the increase in the average grain size and the transformability of the grains resulting from the long isotherm times.

3.3. Statistical Analysis

The results of the statistical analysis carried out using the Tukey test/ANOVA for the flexural strength of the different groups studied in this work are presented in Figure 7a and summarized in Table 3. The Weibull distribution curves are shown in Figure 7b.

Table 3. Comparative statistical analysis (Tukey test/ANOVA) of flexural strength of Y-TZP ceramics.

Sintering Parameter	1475 °C, 2 h	1600 °C, 2 h	1600 °C, 12 h	1600 °C, 24 h
Control Group/1475 °C, 2 h		O	O	O
1600 °C, 2 h			X	O
1600 °C, 12 h				X
1600 °C, 24 h				

X, No significant difference between samples; O, Significant difference between samples.

The results of the Tukey test/ANOVA (Table 3) indicate that the control group ($1475\text{ }^\circ\text{C}$, 2 h) presented values with relevant statistical differences concerning the different groups of samples sintered at $1600\text{ }^\circ\text{C}$, regardless of the adopted level. The samples sintered at $1600\text{ }^\circ\text{C}$ for 2 h presented statistical differences with the $1600\text{ }^\circ\text{C}$ for 24 h group. However, the values are considered without significant statistical differences for the intermediate level ($1600\text{ }^\circ\text{C}$, 12 h). This profile of statistical similarity results from the scattering of results, denoted by the standard deviation values observed in Table 2. On the other hand, even when dealing with ceramic materials, the results of the Weibull statistical analysis (Figure 7b) showed that the highest Weibull modulus (m) values are found in samples sintered at $1475\text{ }^\circ\text{C}$ for 2 h, with $m = 15.0$. These values indicate a microstructure of homogeneous zirconia grains with a monomodal profile, as shown in Figures 5 and 6, and narrow and homogeneous distribution of failures (such as residual micropores), reducing the scatter of flexural strength values.

On the other hand, materials sintered at $1600\text{ }^\circ\text{C}$ for 24 h presented the highest dispersion of results, with flexural strength values ranging from 550 to 1050 MPa (Figure 7b), exhibiting a Weibull modulus, m , of 7.2. There is an interrelation between this significant scattering of results and the crystallographic and microstructural characteristics. The results presented in Figure 6 show that the grain size distribution exhibits a bimodal profile, with a large scattering of sizes, which is related to the difference in the grain growth between t -ZrO₂ and t' -ZrO₂ grains.

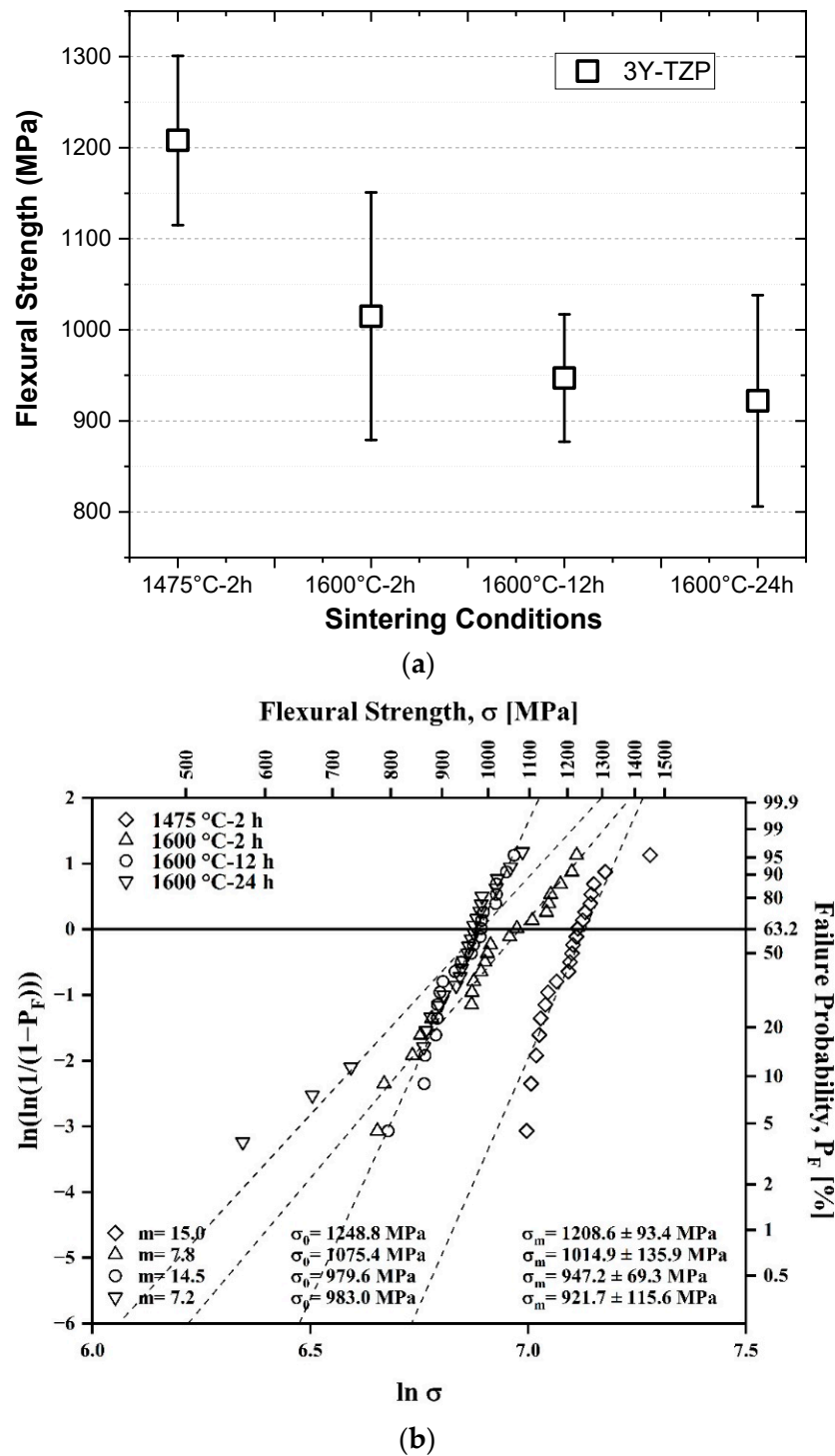


Figure 7. (a) Biaxial flexural strength results for Y-TZP ceramics after sintering. (b) Weibull distributions for groups of Y-TZP ceramics sintered under different conditions.

Considering that the samples were submitted to polishing, and therefore the roughness was very low, the main factor contributing to this strength scatter would be the interfaces between tetragonal and pseudo-cubic (*t'*) ZrO₂ grains located in the critical stress zones to which the samples are subjected during the biaxial bending tests (Figure 7a). In this case, the “pseudo-cubic” (*t'*) grains or grains with little transformability, and thus without toughening capacity observed in this region, cause a larger scattering of the strength values and, therefore, a less reliable material.

According to previous reports, the average flexural strength for Y-TZP ceramics, sintered as recommended by the manufacturer, is between 900 and 1300 MPa [25,30,42,43]. This is in accordance with the flexural strength results reported here, of around 1200 MPa. On the other hand, there is a lack of literature related to quantifying the t' -ZrO₂ and t'' -ZrO₂ phases and their impact on the mechanical properties. One of the few reports available has been made by Vult von Steyern et al. [43]. The authors identified that even a slight increase in the sintering temperature could be related to an increase of the t' -ZrO₂ phase, and consequently, to a reduction in the flexural strength, from ~1250 to ~1050 MPa. Similar behavior has been reported previously by Ruiz and Readey [42], although these authors related their findings to the presence of c -ZrO₂ phase instead of the t' -ZrO₂ phase. Nonetheless, both reports are in accordance with the flexural strength loss reported in this work.

Figure 8 presents the effect of grain size on the flexural strength of Y-TZP ceramics and the quantification of phases of each material, considering transformable and non-transformable ZrO₂ grains.

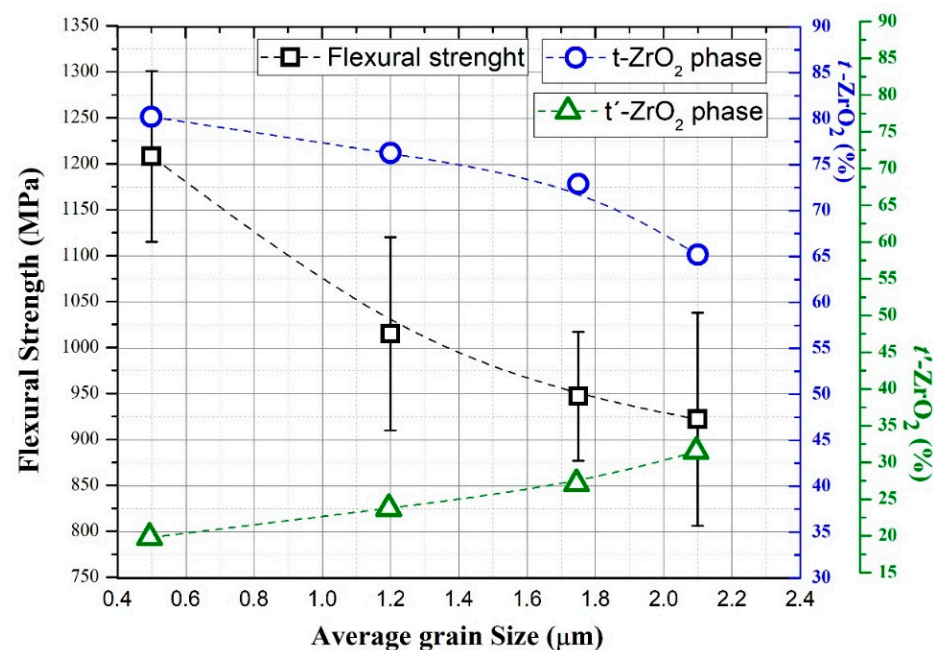


Figure 8. Correlation between average grain size and flexural strength associated with the phase contents of the material.

The analysis of Figure 8 indicates a significant decrease in the flexural strength of the 3Y-TZP ceramic with increasing average grain size. Therefore, the association of the quantification of t and t' -ZrO₂ phase contents with the average grain size and the respective results of flexural strength of zirconia may serve as a guide to understand how the structural characteristics of 3Y-TZP ceramics influence the bending strength.

According to a previous study by Shukla et al. [12], ZrO₂-tetragonal grains on the sub-micrometer scale (0.1~1 μm) have the most favorable conditions to enable the transformability, $t \rightarrow m$, during crack propagation and consequently to increase the strength. This interpretation explains the behavior found in this investigation for samples sintered at 1475 °C for 2 h, which have an average grain size of 0.65 μm. However, as identified by Krogstad et al. [39] and detected in this work, there is a correlation between transformable (t) and non-transformable (t') grains in 3Y-TZP ceramics, which in the case of samples sintered at 1475 °C for 2 h, is 80.2% of transformable grains (t -ZrO₂) and 19.8% of t' -ZrO₂ grains, well-dispersed and without significant size differences between them. In this case, the shielding zones at the crack tip are more concentrated and effective, favoring the shielding of propagating cracks and improving their resistance.

There was a considerable increase in the average grain size (greater than 1 μm) by increasing the sintering temperature. It was also observed that the growth of a discrete population of zirconia grains, which we refer to as non-transformable t' -ZrO₂ grains, led to the loss of effectiveness of the shielding zone at the crack tip. These non-transformable grains also reduce the strength of the ceramic. The recurrent diffusional effects during grain growth are accentuated for longer dwell times, directly reflecting the average growth of transformable (t -ZrO₂) and non-transformable (t' -ZrO₂) grains. Due to its higher concentration, the increase in grains (t') decreases the toughening capacity and fracture resistance of 3Y-TZP ceramics.

4. Conclusions

In 3Y-TZP ceramics, increasing the final sintering temperature and the dwell time led to a considerable decrease in flexural strength. Samples sintered at 1475 °C for 2 h showed flexural strength values of 1208 ± 93 MPa, while groups sintered at 1600 °C for 2 or 24 h showed mean strength values of 1015 ± 136 MPa (15.9% reduction) and 922 ± 116 MPa (23.7% reduction), respectively. This behavior is related to the growth of tetragonal ZrO₂ grains and, in particular, associated with the progressive formation of “pseudo-cubic” (t' -ZrO₂) tetragonal grains, with low tetragonality, caused by the grain boundary segregation-induced phase (GBSIPT) mechanism.

The amount of t' -ZrO₂ grains increased as a function of sintering temperature and dwell time. Due to their high concentration of stabilizer in solid solution, these grains have lower tetragonality, being extremely stable at room temperature and not undergoing the martensitic transformation ($t \rightarrow m$) under mechanical stress. Therefore, they limit the effectiveness of shielding zones at the crack tip and reduce the effects of phase transformation toughening.

Author Contributions: Conceptualization, M.F.R.P.A. and C.d.S.; methodology, M.F.R.P.A., L.Q.B.d.C. and B.G.S.; software, M.F.R.P.A., L.Q.B.d.C. and B.G.S.; validation, C.d.S., C.R.M.d.S. and K.S.; formal analysis, M.F.R.P.A., K.S. and C.d.S.; investigation, M.F.R.P.A., L.Q.B.d.C. and C.d.S.; resources, M.F.R.P.A. and C.d.S.; data curation, M.F.R.P.A., B.G.S. and C.d.S.; writing—original, M.F.R.P.A., K.S. and C.d.S.; draft preparation, M.F.R.P.A. and B.G.S.; writing—review and editing, C.d.S., C.R.M.d.S. and K.S.; visualization, C.d.S., M.F.R.P.A. and K.S.; supervision, C.d.S.; project administration, C.d.S. and M.F.R.P.A.; funding acquisition, C.d.S. All authors have read and agreed to the published version of the manuscript.

Funding: This research was funded by Fundação Carlos Chagas Filho de Amparo à Pesquisa do Estado do Rio de Janeiro (FAPERJ), Grant Nos. E26-201.476/2014 and E26-202.997/2017, and Conselho Nacional de Desenvolvimento Científico e Tecnológico (CNPq), Grant No. 311119/2017-4.

Institutional Review Board Statement: Not applicable.

Informed Consent Statement: Not applicable.

Data Availability Statement: Not applicable.

Conflicts of Interest: The authors declare no conflict of interest. The funders had no role in the design of the study, in the collection, analyses, or interpretation of data, in the writing of the manuscript, or in the decision to publish the results.

References

1. Kelly, J.R.; Denry, I. Stabilized zirconia as a structural ceramic: An overview. *Dent. Mater.* **2008**, *24*, 289–298. [[CrossRef](#)] [[PubMed](#)]
2. Manicone, P.F.; Iommetti, P.R.; Raffaelli, L. An overview of zirconia ceramics: Basic properties and clinical applications. *J. Dent.* **2007**, *35*, 819–826. [[CrossRef](#)]
3. Stevens, R. *An Introduction to Zirconia: Zirconia and Zirconia Ceramics*, 2nd ed.; Magnesium Electrum: Twickenham, UK, 1986.
4. Basu, B. Toughening of yttria-stabilized tetragonal zirconia ceramics. *Int. Mater. Rev.* **2005**, *50*, 239–256. [[CrossRef](#)]
5. Kelly, P.M.; Rose, L.F. The martensitic transformation in ceramics—Its role in transformation toughening. *Prog. Mater. Sci.* **2002**, *47*, 463–557. [[CrossRef](#)]
6. Lange, F.F. Transformation toughening. *J. Mater. Sci.* **1982**, *17*, 225–234. [[CrossRef](#)]

7. Matsui, K.; Yoshida, H.; Ikuhara, Y. microstructure-development mechanism during sintering in polycrystalline zirconia. *Int. Mater. Rev.* **2018**, *63*, 375–406. [[CrossRef](#)]
8. Ruhle, M.; Claussen, N.; Heuer, A.H. Microstructural studies of Y₂O₃-containing tetragonal ZrO₂ polycrystals (Y-TZP). In *Science and Technology of Zirconia II*; American Ceramic Society, Inc.: Columbus, OH, USA, 1983.
9. Basu, B.; Vleugels, J.; Van Der Biest, O. Transformation behavior of tetragonal zirconia: Role of dopant content and distribution. *Mater. Sci. Eng. A* **2004**, *366*, 338–347. [[CrossRef](#)]
10. Yashima, M.; Kakihana, M.; Yoshimura, M. Metastable-stable phase diagrams in the zirconia-containing systems utilized in solid-oxide fuel cell application. *Solid State Ion.* **1996**, *86*, 1131–1149. [[CrossRef](#)]
11. Viazzi, C.; Bonino, J.P.; Ansart, F.; Barnabé, A. Structural study of metastable tetragonal YSZ powders produced via a sol-gel route. *J. Alloys Compd.* **2008**, *452*, 377–383. [[CrossRef](#)]
12. Shukla, S.; Seal, S. Phase Stabilization in Nanocrystalline Zirconia. *Rev. Adv. Mater. Sci.* **2003**, *5*, 117–120.
13. Shahmiri, R.; Standard, O.C.; Hart, J.N.; Sorrell, C.C. Optical properties of zirconia ceramics for esthetic dental restorations: A systematic review. *J. Prosthet. Dent.* **2018**, *119*, 36–46. [[CrossRef](#)] [[PubMed](#)]
14. Zhang, F.; Inokoshi, M.; Batuk, M.; Hadermann, J.; Naert, I.; Van Meerbeek, B.; Vleugels, J. Strength, toughness and aging stability of highly-translucent Y-TZP ceramics for dental restorations. *Dent. Mater.* **2016**, *32*, e327–e337. [[CrossRef](#)] [[PubMed](#)]
15. Egilmez, F.; Ergun, G.; Cekic-Nagas, I.; Vallittu, P.K.; Lassila, L.V. Factors affecting the mechanical behavior of Y-TZP. *J. Mech. Behav. Biomed. Mater.* **2014**, *37*, 78–87. [[CrossRef](#)] [[PubMed](#)]
16. Sakuma, T.; Yoshizawa, Y. The grain growth of zirconia during annealing in the cubic/tetragonal two-phase region. *Mater. Sci. Forum* **1992**, *94*, 865–870. [[CrossRef](#)]
17. Ramesh, S.; Lee, K.S.; Tan, C.Y. A review on the hydrothermal ageing behavior of Y-TZP ceramics. *Ceram. Int.* **2018**, *44*, 20620–20634. [[CrossRef](#)]
18. Theunissen, G.S.A.M.; Bouma, J.S.; Winnubst, A.J.A.; Burggraaf, A.J. Mechanical properties of ultra-fine grained zirconia ceramics. *J. Mater. Sci.* **1992**, *27*, 4429–4438. [[CrossRef](#)]
19. *ISO 6872; Dentistry Ceramic Materials*. 4th ed. International Organization for Standardization: Geneva, Switzerland, 2015; pp. 1–14.
20. Hill, R.J. Expanded use of the Rietveld method in studies of phase abundance in multiphase mixtures. *Powder Diffr.* **1991**, *6*, 74–77. [[CrossRef](#)]
21. Rodriguez-Carvajal, J. *Computer Program FullProf, Version 3.51*; Laboratoire Leon Brillouin, CEA-CNRS: Grenoble, France, 1998.
22. Krogstad, J.A.; Lepple, M.; Gao, Y.; Lipkin, D.M.; Levi, C.G. Effect of yttria content on the zirconia unit cell parameters. *J. Am. Ceram. Soc.* **2011**, *94*, 4548–4555. [[CrossRef](#)]
23. Yashima, M.; Ishizawa, N.; Yoshimura, M. High-Temperature X-ray Study of the Cubic-Tetragonal Diffusionless Phase Transition in the ZrO₂-ErO_{1.5} System: I, Phase Change between Two Forms of a Tetragonal Phase, t'-ZrO₂, and t''-ZrO₂, in the Compositionally Homogeneous 14 mol% ErO_{1.5}-ZrO₂. *J. Am. Ceram. Soc.* **1993**, *76*, 641–648. [[CrossRef](#)]
24. Yashima, M.; Sasaki, S.; Kakihana, M.; Yamaguchi, Y.; Arashi, H.; Yoshimura, M. Oxygen-induced structural change of the tetragonal phase around the tetragonal-cubic phase boundary in ZrO₂-YO_{1.5} solid solutions. *Acta Crystallogr. Sect. B Struct. Sci.* **1994**, *50*, 663–672. [[CrossRef](#)]
25. Jue, J.F.; Chen, J.; Virkar, A.V. Low-temperature aging of t'-zirconia: The role of microstructure on phase stability. *J. Am. Ceram. Soc.* **1991**, *74*, 1811–1820. [[CrossRef](#)]
26. Fabregas, I.O.; Reinoso, M.; Otal, E.; Kim, M. Grain-size/(t'' or c)-phase relationship in dense ZrO₂ ceramics. *J. Eur. Ceram. Soc.* **2016**, *36*, 2043–2049. [[CrossRef](#)]
27. Bučevac, D.; Kosmač, T.; Kocjan, A. The influence of yttrium-segregation-dependent phase partitioning and residual stresses on the aging and fracture behaviour of 3Y-TZP ceramics. *Acta Biomater.* **2017**, *62*, 306–316. [[CrossRef](#)] [[PubMed](#)]
28. Matsui, K.; Nakamura, K.; Kumamoto, A.; Yoshida, H.; Ikuhara, Y. Low-temperature degradation in yttria-stabilized tetragonal zirconia polycrystal doped with small amounts of alumina: Effect of grain-boundary energy. *J. Eur. Ceram. Soc.* **2016**, *36*, 155–162. [[CrossRef](#)]
29. Wei, C.; Gremillard, L. Towards the prediction of hydrothermal ageing of 3Y-TZP bioceramics from processing parameters. *Acta Mater.* **2018**, *144*, 245–256. [[CrossRef](#)]
30. Camposilvan, E.; Leone, R.; Gremillard, L.; Sorrentino, R.; Zarone, F.; Ferrari, M.; Chevalier, J. Aging resistance, mechanical properties and translucency of different yttria-stabilized zirconia ceramics for monolithic dental crown applications. *Dent. Mater.* **2018**, *34*, 879–890. [[CrossRef](#)]
31. *ASTM E1876-15; Standard Test Method for Dynamic Young's Modulus, Shear Modulus, and Poisson's Ratio by Impulse Excitation of Vibration*. ASTM International: West Conshohocken, PA, USA, 2015; pp. 1–17.
32. Niihara, K.; Morena, R.; Hasselman, D.P.H. Evaluation of K_{IC} of brittle solids by the indentation method with low crack-to-indent ratios. *J. Mater. Sci. Lett.* **1982**, *1*, 13–16. [[CrossRef](#)]
33. Shetty, D.K.; Rosenfield, A.R.; Duckworth, W. Analysis of indentation crack as a wedge-loaded half-penny crack. *J. Am. Ceram. Soc.* **1985**, *68*, C-65–C-67. [[CrossRef](#)]
34. Ćorić, D.; Renjo, M.M.; Ćurković, L. Vickers indentation fracture toughness of Y-TZP dental ceramics. *Int. J. Refract. Met. Hard Mater.* **2017**, *64*, 14–19. [[CrossRef](#)]
35. Weibull, W. A statistical distribution function of wide applicability. *J. Appl. Mech.* **1951**, *18*, 290–293. [[CrossRef](#)]

36. Shapiro, S.S.; Wilk, M.B. An analysis of variance test for normality (complete samples). *Biometrika* **1965**, *52*, 591–611. [[CrossRef](#)]
37. Mohr, D.L.; Wilson, W.J.; Freund, R.J. *Statistical Methods*, 4th ed.; Elsevier Inc.: Amsterdam, The Netherlands, 2022; 767p.
38. Chevalier, J.; Gremillard, L.; Virkar, A.V.; Clarke, D.R. The tetragonal-monoclinic transformation in zirconia: Lessons learned and future trends. *J. Am. Ceram. Soc.* **2009**, *92*, 1901–1920. [[CrossRef](#)]
39. Krogstad, J.A.; Gao, Y.; Bai, J.; Wang, J.; Lipkin, D.M.; Levi, C.G. In situ diffraction study of the high-temperature decomposition of t'-zirconia. *J. Am. Ceram. Soc.* **2015**, *98*, 247–254. [[CrossRef](#)]
40. Djurado, E.; Bouvier, P.; Lucazeau, G. Crystallite size effect on the tetragonal-monoclinic transition of undoped nanocrystalline zirconia studied by XRD and Raman spectrometry. *J. Solid State Chem.* **2000**, *149*, 399–407. [[CrossRef](#)]
41. Gibson, I.R.; Irvine, J.T. Qualitative X-ray Diffraction Analysis of Metastable Tetragonal (t') Zirconia. *J. Am. Ceram. Soc.* **2001**, *84*, 615–618. [[CrossRef](#)]
42. Ruiz, L.; Readey, M.J. Effect of heat treatment on grain size, phase assemblage, and mechanical properties of 3 mol% Y-TZP. *J. Am. Ceram. Soc.* **1996**, *79*, 2331–2340. [[CrossRef](#)]
43. Von Steyern, P.V.; Bruzell, E.; Vos, L.; Andersen, F.S.; Ruud, A. Sintering temperature accuracy and its effect on translucent yttria-stabilized zirconia: Flexural strength, crystal structure, tetragonality and light transmission. *Dent. Mater.* **2022**, *38*, 1099–1107. [[CrossRef](#)]